Intramolecular Dynamics of RS−SR′ Systems (R, R′ = H, F, Cl, CH_3, C_2H_5): Torsional Potentials, Energy Levels, Partition Functions†

Vincenzo Aquilanti,*,‡ Mirco Ragni,‡ Ana C. P. Bitencourt,‡,⊥ Glauciete S. Maciel,‡ and Frederico V. Prudente§

Dipartimento di Chimica, Università di Perugia, 06123 Perugia, Italy, and Instituto de Física, Universidade Federal da Bahia, 40210-340 Salvador, Bahia, Brazil

Received: October 24, 2008; Revised Manuscript Received: December 17, 2008

The equilibrium and cis and trans geometric structures of a series of disulfides RS−SR′ (HSSH, HSSF, HSSCl, $HSSCH_3$, $HSSC_2H_5$, FSSF, ClSSCl, ClSSF, CH_3SSCH_3, $C_2H_5SSC_2H_5$) have been studied using both density functional theory (B3LYP/6-311++G(3df, 3pd)) and second-order Møller−Plesset perturbation theory (MP2(FU)/aug-cc-pVTZ). The effects of internal rotation on the structural parameters have been analyzed and the torsional potentials around the S−S bond have been compared with experimental and theoretical information, when available, as well as with the analogues of the peroxydic family. Torsional levels were calculated, and their distribution as a function of temperature was determined, obtaining partition functions. This information is of interest for statistical approaches to equilibrium properties and to rates of processes in which torsional anharmonicity is relevant. It is also required for recent atmospheric modeling studies and also for prototypical chiral separation experiments, in view of a possible dynamic mechanism for chirality exchange by molecular collisions. In general, barriers for such processes are higher than for the corresponding peroxides, and accordingly, rates for chirality change are estimated to be consistently smaller.

Introduction

In recent years, disulfides have been investigated with increasing interest due to their importance in biochemistry and atmospheric processes.[1−4] The biological activity of several molecules, such as proteins, enzymes, and antibiotics, are characterized by the presence of the disulfide linkage. A number of experimental[5−9] and theoretical studies[10−23] of the structural and energetic aspects of several disulfide molecules have been performed and provide useful information on the electronic mechanism involved in the S−S bond cleavage.

We are interested, in general, in the conformational and energetic properties of molecules containing O−O and S−S bonds. Studies by quantum mechanical methods for hydrogen peroxide (H_2O_2) and its derivatives were performed with the purpose of elucidating the features of the internal modes and, in particular, the torsion around the O−O and S−S bonds which leads to the chirality changing isomerization.[24−29]

Although there is a large amount of data available for H_2O_2 (see ref 4 and references therein) much less information is available for H_2S_2 (its analogue with a heavier atom) and its derivatives. In view of the possible importance of results obtained for the prototypical disulfide molecule, H_2S_2, with respect to the effect of level of theory and basis sets used to obtain electronic properties (dipole moments, polarizability) and geometrical parameters, a detailed analysis was done for this molecule in a previous paper.[29] Regarding intermolecular interactions, of specific importance for collisional chirality exchange, a study was performed for both H_2O_2−rare gas[27] and H_2S_2−rare gas[29] systems, for which information should also come from molecular beam experiments in our laboratory. This will extend to these systems the joint experimental and theoretical approach already tackled for interactions of H_2O[30,31] and H_2S[32,33] with the rare gases.

In the present paper, we report the effects of the substitution of one or both hydrogens in hydrogen persulfide (HSSH) by halogen atoms or alkyl groups studied by a detailed investigation of the geometries, dipole moments, and cis and trans barriers as well as a comparison of available experimental and theoretical data. Attention has also been dedicated to a study of energy levels in the very anharmonic torsional potentials, obtaining their distributions as a function of temperature. This also permits the calculation of partition functions for the torsional motion, of relevance for the isomerization rate leading to exchange between chiral enantiomers. Partition functions are obtained both by direct summation over calculated levels and by classical and semiclassical approaches, whose accuracy is discussed. Estimated rates both for underbarrier tunneling and overbarrier transition are presented and shown to be consistently smaller than for the corresponding O−O cases due to the generally higher barriers.[28]

The next section outlines the quantum chemical computational aspects. Section 3 presents and discusses results on the torsional energy profiles. In Section 4, torsional levels, partition functions and racemization rates are reported. Further remarks and conclusions follow in Section 6.

2. Computational Methods

All the calculations have been carried out using the Gaussian 03 package.[34] The torsional potential of several disulfides has been determined by MP2(FU)/aug-cc-pVTZ and B3LYP/6-311++G (3df,3pd) methods and is shown in Figure 1, Figure 2, and Figure 3. The DFT methodology is particularly attractive

† Part of the "George C. Schatz Festschrift".

* Corresponding author. E-mail: aquila@dyn.unipg.it.

‡ Dipartimento di Chimica, Università di Perugia, 06123 Perugia, Italy

§ Instituto de Física, Universidade Federal da Bahia, 40210-340 Salvador, Bahia, Brazil

⊥ Present address: Centro de Formação de Professores, Universidade Federal do Recôncavo da Bahia, Amargosa, Brazil

10.1021/jp8094215 CCC: $40.75
Published on Web 01/30/2009

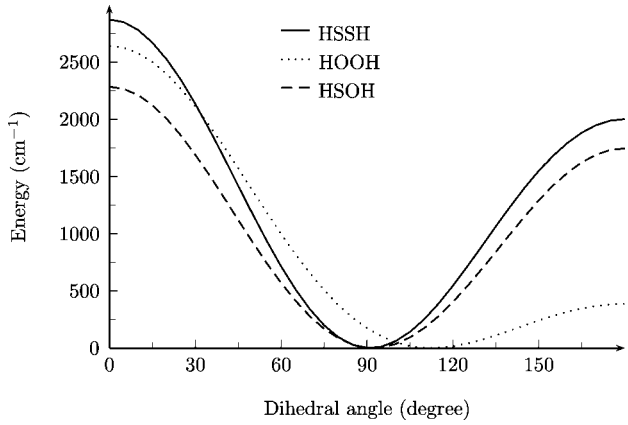

Figure 1. Profiles of the torsional potentials for HSSH, HOOH, and HSOH as a function of dihedral angle for the optimized calculations with the MP2(FU)/aug-cc-pvtz method.

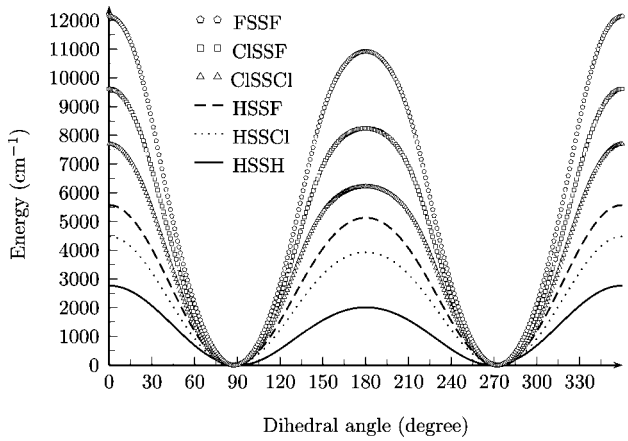

Figure 2. Profiles of the torsional potentials for the halogen disulfides as a function of dihedral angle from the optimized calculations with the B3LYP/6-311++G(3df,3pd) method.

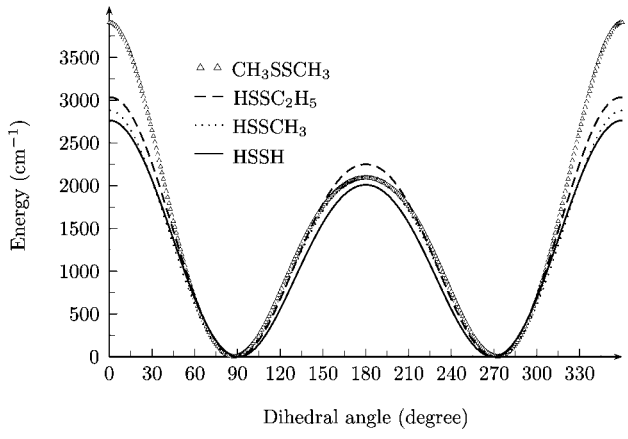

Figure 3. Profiles of the torsional potentials for the alkyl disulfides as a function of dihedral angle from the optimized calculations with the B3LYP/6-311++G(3df,3pd) method.

for alkyl derivatives because of its formal N^4 scaling (N = number of basis functions), reducing the computational cost, when the number of involved atoms increases. The equilibrium geometric structure for RSSR′ series has been determined for both B3LYP/6-311++G(3df,3pd) and MP2(FU)/aug-cc-pVTZ. Table 1 shows the difference between barriers for ROOR′ and RSSR′ systems using B3LYP/6-311++G(3df,3pd). The geometric parameters, barriers, and dipole moments for the three main configurations (cis, trans, and equilibrium) are listed in Table 2 using MP2(FU)/aug-cc-pVTZ. Comparison with available experimental and theoretical results are also reported.

TABLE 1: Cis and Trans Barriers (cm^{-1}) for ROOR′ and RSSR′ Molecules at the B3LYP/6-311++G (3df,3pd) Level

ROOR′[28]	cis	trans	RSSR′	cis	trans
HOOH[a]	2575.5	386.3	HSSH	2764.4	2009.9
HOOF[b]	3338.7	3542.2	HSSF	5562.3	5131.2
HOOCl[b]	2317.8	1617.8	HSSCl	4481.5	3929.5
ClOOCl[b]	3523.7	2166.8	ClSSCl	7969.3	6218.3
ClOOF[b]	6037.5	4718.4	ClSSF	9617.5	8252.5
FOOF[b]	9728.5	8304.0	FSSF	12144.5	10923.0
$HOOCH_3$[c]	2080.0	151.9	$HSSCH_3$	2881.4	2107.5
$HOOC_2H_5$[c]	2270.6	236.5	$HSSC_2H_5$	3030.0	2248.7
CH_3OOCH_3[c]	3904.4	0.0	CH_3SSCH_3	4008.2	2094.0
$C_2H_5OOC_2H_5$[c]	4365.7	0.0	$C_2H_5SSC_2H_5$		2451.8

[a] See ref 24. [b] See ref 26. [c] See ref 25.

Atomic partial charges were calculated by the Merz−Kollman model[35] and are shown in Figure 4. This method was chosen on the basis of previous experience (see, e.g., ref 36), demonstrating its adequacy to describe electrostatic properties at relatively low computational cost.

3. Torsional Energy Profiles

Figure 1 shows the torsional modes around three different bonds: O−O (hydrogen peroxide), S−S (hydrogen persulfide), and O−S (hydrogen thioperoxide). About HOOH and HSSH, see refs 25 and 29, respectively. The HOSH molecule is included in this study because its radicals are involved in various processes associated with the atmospheric oxidation of sulfides, one of the chemical processes that leads to acid rain and the depletion of ozone.[1]

From these plots, it is possible to see that, although HOOH has an equilibrium dihedral angle of 112°, even a single S atom shifts this angle toward 90°. Figures 2 and 3 show, for equilibrium geometries, the same dihedral angles of ∼90° independent of the kind of substituent used. Another characteristic behavior is the "symmetry" observed between cis and trans barriers. Although HSSH and HOSH have a qualitatively similar profile, the trans barrier of HOOH is very small when compared with its cis barrier.

Halogen Disulfides. Figure 2 shows that the heights of cis and trans barriers vary appreciably with the nature of the substituent and increase with its electronegativity. The graph shows also that the presence of a single halogen atom practically doubles the cis barrier height with respect to that of HSSH. Further substitution by another halogen has a similar effect. The sensitivity to substitution on the values for barrier heights can be seen from data in Table 1, where comparison is also made with the analogous cases for halogen substitution in HOOH.[27]

As can be seen in Figure 2 and Table 1, the mono- and disubstituted chloro compounds present lower barriers than do their fluoro analogues, both for peroxides and for persulfides. Those of the latter are consistently several times higher than those of the former. In all cases except HOOF (see ref 26), trans barriers are lower than cis ones so that racemization is expected to proceed essentially via a route involving the trans barrier. Existing experimental information for peroxides is discussed in refs 25 and 26, and it is not available for persulfides.

The increase in the calculated barriers for FSSF, accompanied by the shortening of the S−S bond (Table 2), has been attributed to the two hyperconjugated interactions between the lone pair of 3p free electrons for each sulfur atom.[7,37] They are partially

TABLE 2: Geometries, Barriers and Dipole Moments μ (D) for the RSSR′ Molecules at the MP2(FU)/aug-cc-pVTZ Level[a]

RSSR′	r_{RS}	$r_{SR'}$	r_{SS}	$\hat{R}SS$	$\hat{S}SR'$	RSSR′	barriers	μ
HSSH[b]	1.345	1.345	2.058	98.1	98.1	90.8		1.17
eq	1.336	1.336	2.059	97.7	97.7	91.1		1.25
cis	1.332	1.332	2.111	96.1	96.1	0.0	2873.36	1.25
trans	1.336	1.336	2.102	92.4	92.4	180.0	2003.08	1.72
HSSF[c]	1.355	1.659	2.009	100.3	104.4	87.3		
eq	1.340	1.642	1.991	99.3	103.6	87.6		1.94
cis	1.335	1.628	2.102	90.5	98.9	0.0	5490.93	0.74
trans	1.338	1.625	2.089	90.4	95.6	180.0	5020.90	2.13
HSSCl[c]	1.353	2.092	2.092	99.6	106.8	87.2		
eq	1.339	2.051	2.013	98.3	105.0	86.8		1.55
cis	1.333	2.022	2.110	93.1	101.6	0.0	4564.59	0.63
trans	1.338	2.021	2.096	91.3	96.7	180.0	3966.94	1.55
$HSSCH_3$[d]								1.95
eq	1.338	1.803	2.047	98.2	101.2	88.0		1.89
cis	1.334	1.796	2.100	95.2	99.3	0.0	2863.75	2.49
trans	1.335	1.798	2.091	93.8	94.6	180.0	2048.27	0.93
$HSSC_2H_5$[d]								1.96
eq	1.342	1.819	2.056	98.7	101.9	88.98		2.03
trans	1.339	1.814	2.101	93.8	95.3	180.0	2253.89	1.13
FSSF[e]	1.635	1.635	1.890	108.3	108.3	87.7		
eq	1.644	1.644	1.894	107.9	107.9	87.7		1.75
cis	1.615	1.615	2.155	97.7	97.7	0.0	12095.32	2.05
trans	1.627	1.627	2.108	93.2	93.2	180.0	10655.46	0
ClSSCl[f]	2.055	2.055	1.950	107.7	107.7	85.2		
eq	2.056	2.056	1.955	106.8	106.8	85.0		0.95
cis	2.002	2.002	2.155	104.5	104.5	0.0	6916.26	0.48
trans	2.024	2.024	2.095	94.4	94.4	180.0	5194.92	0
ClSSF								
eq	1.923	1.640	2.069	108.4	106.4	86.8		1.41
cis	2.001	1.615	2.151	100.9	100.9	0.0	9131.44	1.24
trans	2.097	1.627	2.024	97.1	89.4	180.0	7342.92	0.77
CH_3SSCH_3[f,g]	1.810	1.810	2.038	102.8	102.8	84.7		2.41
eq	1.813	1.813	2.046	101.6	101.6	84.4		2.26
trans	1.807	1.807	2.090	96.1	96.1	180.0	1968.29	0
$C_2H_5SSC_2H_5$[b]	1.832	1.832	2.038	103.7	103.7	90		
eq	1.838	1.838	2.052	104.2	104.2	88.6		2.19
trans	1.826	1.826	2.111	98.0	98.0	180.0		
HSOH[h]	1.373	0.978	1.677	105.7	99.8			
eq	1.337	0.962	1.674	106.7	98.0	92.0		
cis	1.330	0.963	1.696	105.3	92.8	0.0	2203.89	
trans	1.335	0.961	1.692	108.7	99.2	180.0	1504.04	

[a] Distances in Å, angles in degrees, and energies in cm^{-1}. [b] Experimental data, ref 4. [c] Theory, ref 22. [d] Experimental dipole moments, ref 61. [e] Theory, ref 6. [f] Theory, ref 7. [g] Experimental dipole moments, ref 16. [h] Theory, ref 14.

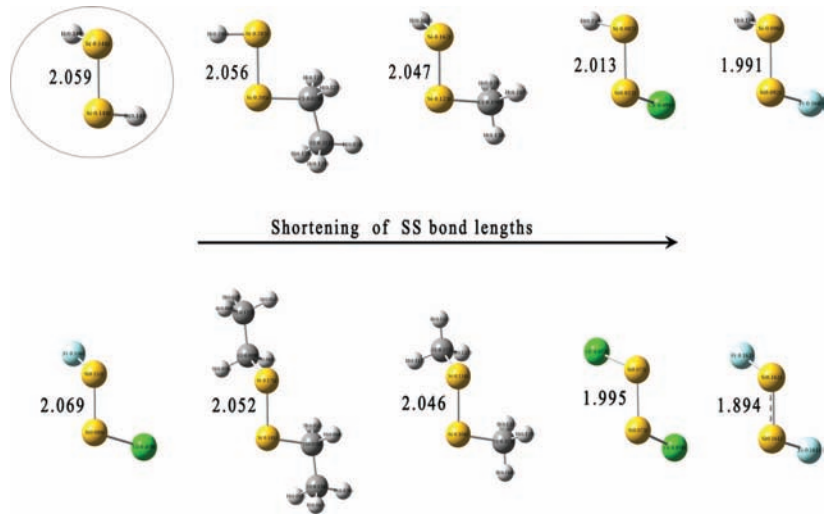

Figure 4. Merz−Kollman atomic partial charges and S−S bond lengths for several disulfides calculated at the MP2(FU)/aug-cc-pVTZ level.

delocalized into the antibonding orbital σ^*S−F, the delocalization being greatest for a gauche configuration.[4]

Alkyl Disulfides. Comparison of the results obtained for HSSH and for its alkyl derivatives suggests that inclusion of the alkyl groups increases in a significant way the barrier heights only for double substitution, as for CH_3SSCH_3. The other compounds of the series appear not to have large enough "volume" to influence the barrier heights. It is interesting to

TABLE 3: Equilibrium Geometries, Cis and Trans Barriers Calculated with the B3LYP//6-311 ++G(3df,3pd) Method and with Fitting (eq 1)[a]

molecule	r_{RS}	r_{SS}	$r_{SR'}$	R̂SS	ŜSR′	dihedral	cis	cis-fit	trans	trans-fit
HSSH DFT	1.347	2.074	1.347	98.651	98.651	90.735	2764.35	2765.16	2009.86	2010.18
HSSH MP2	1.336	2.058	1.336	97.708	97.708	91.091	2873.36	2871.72	2003.08	2001.63
HSSF	1.353	2.001	1.653	100.533	104.575	87.576	5562.34	5582.67	5131.21	5137.10
HSSCl	1.351	2.021	2.084	99.758	107.063	87.161	4481.47	4487.39	3929.45	3933.36
ClSSCl	2.098	1.949	2.098	109.515	109.515	87.203	7696.32	7708.78	6218.26	6199.41
ClSSF	2.113	1.923	1.651	110.476	107.675	87.675	9617.53	9650.31	8252.53	8241.28
FSSF	1.657	1.902	1.657	108.617	108.617	87.783	12144.46	12215.15	10922.99	10926.86
$HSSCH_3$	1.349	2.064	1.820	99.3018	103.420	87.834	2881.42	2878.89	2107.46	2105.66
$HSSC_2H_5$	1.348	2.065	1.832	99.6561	104.044	89.450	3030.00	3047.80	2248.71	2255.50

[a] The bond lengths are expressed in Å, the angles in degrees, and the barriers in cm^{-1}. In particular, the HSSH system was studied also with the MP2/aug-cc-pVTZ method.

TABLE 4: Parameters α (see eqs 4 and 5) and Coefficients of $V(\varphi)$ (see eq 1)

	α, cm^{-1}		coefficients of the fitting, cm^{-1}						
systems	α_0	α_1	V_0	V_1	V_2	V_3	V_4	V_5	rmsd
HSSH DFT	19.5822	0.127192	1210.345	291.202	1194.308	82.475	−16.981	3.812	0.600
HSSH MP2	19.8104	0.113589	1230.584	342.289	1217.162	89.078	−11.075	3.678	1.191
HSSF	10.4853	0.189175	2699.828	9.257	2679.614	193.889	−19.558	19.636	6.591
HSSCl	10.1596	0.191991	2125.280	56.352	2103.198	196.727	−18.106	23.937	3.936
ClSSCl[a]	0.775347	0.263031	3533.332	175.712	3541.192	467.437	−43.363	120.889	12.033
ClSSF[b]	1.10878	0.285471	4469.346	90.488	4574.870	459.677	21.115	154.401	19.956
FSSF[c]	1.44926	0.303202	5637.086	12.382	5900.878	460.659	176.747	168.735	39.692
$HSSCH_3$	10.4161	0.157707	1259.245	217.725	1243.775	156.028	−10.747	12.862	1.208
$HSSC_2H_5$	10.278	0.16556	1346.505	273.531	1327.422	118.232	−22.275	4.387	3.897

[a] $C_6 = -77.066$ cm^{-1} and $C_7 = -9.358$ cm^{-1}. [b] $C_6 = -119.536$ cm^{-1} and $C_7 = -0.052$ cm^{-1}. [c] $C_6 = -143.706$ cm^{-1} and $C_7 = 2.371$ cm^{-1}.

note that in the corresponding ROOR′ systems,[25] even a single methyl or ethyl group substitution leads to the lowering of both barriers with respect to HOOH (see Table 1 and ref 25), and double substitution gives rise to an increase of the cis barriers and disappearance of the trans barriers. In view of the higher S−S distances as compared to the O−O ones in these series of compounds, it is reasonable to expect here a lower role of steric effects.

In Figure 3 and especially in Table 1, it can be noted that monosubstitution of the hydrogen in HSSH does not alter significantly the heights for both barriers, but disubstitution increases the cis barrier height correspondingly to the "size" of the alkyl group.

Summarizing the discussion of differences between the effect of substitution on peroxides and persulfides, the main one is on the trans barrier, which by alkyl substitution is practically unaffected in H_2S_2 but drastically decreases for H_2O_2.[25]

Structural Aspects. The relative stabilities as well as isomerizations between RSSR and $R_2S{=}S$ (R = H, F, Cl, and alkyl) have received some interest but still remain controversial (see ref 4 and references therein). For FSSF and $F_2S{=}S$, see refs 11 and 21, and for ClSSCl, see ref 17. Here, we limit our study to RSSR′ structures.

The geometrical parameters of the disulfides are substantially influenced by the presence of electronegative atoms. In both theoretical and experimental data, we found that for the molecules with single and double halogen substitutions (HSSF, HSSCl, FSSF, and ClSSCl), the S−S bond lengths decrease for increasing electronegativity of the substituent, whereas the S−F and S−Cl bond lengths increase (see Table 2). An exception is observed for ClSSF, in which the S−S bond length is 0.01 Å larger than in the HSSH molecule. From Table 2, one can see that decreases in the SS bond lengths correspond to increases in RS bond lengths, the effects being much larger for SS than for RS. In general, for the F−S bond, the increase is 0.30 Å, whereas for S−Cl, it is 0.71 Å. For all disulfide compounds, the dihedral angles are 2−4° lower than HSSH, and SSR bond angles increase by 3−7° for monohalodisulfides and by 8−10° for dihalodisulfides. In the alkyl disulfides, a variation of the SSR angle is very small as the substituent group size increases (∼0.6°) and similarly is small for the passage from single to double substitution.

Charge Distribution, S−S Bond Lengths and Barrier Heights. According to an analysis of the distribution of charges, obtained following the Merz−Kollman approach,[35] for the RSSR′ series, we observe that the shortening of the SS bond lengths is associated with an increase in the positive charge on the sulfur atom (see Figure 4). As already noted, such a shortening does not show up in ClSSF, where, in contrast, the SS bond is slightly larger. Dolenko et al.[7] reported that the growth of the geminal $n_s - \sigma^*SX$ conjugation efficiency leads to the shortening of the SS bond that is more than 2−4 times larger than the simultaneous SX bond lengthening. In general, such a shortening appears to be correlated to the increase in barrier heights, an extreme case being that of FSSF (Table 2).

4. Torsional Levels, Partition Functions, Racemization Rates

In this section, we extend to disulfides our study of intramolecular dynamics applied in a recent paper to H_2O_2 and its derivatives.[28] For that series of molecules, a systematic quantum chemical investigation had been carried out.[24−26] The emphasis has been on the characterization of the torsional mode, which is responsible for the stereomutation; namely the exchange between chiral enantiomers through the trans and cis barriers, a motivation being the understanding of the possible role of a

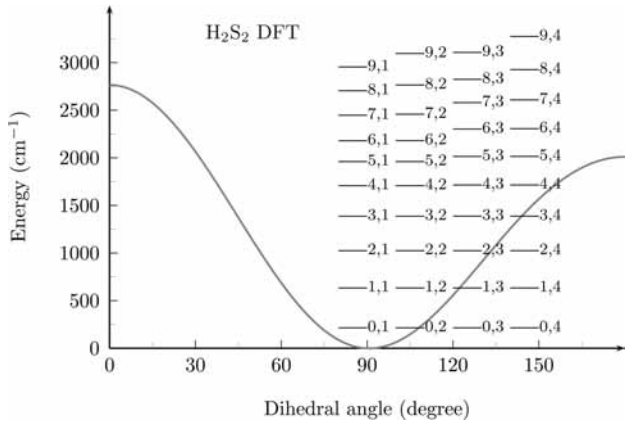

Figure 5. Torsional energy profile as a function of the dihedral angle and energy levels n and τ for HSSH (B3LYP method).

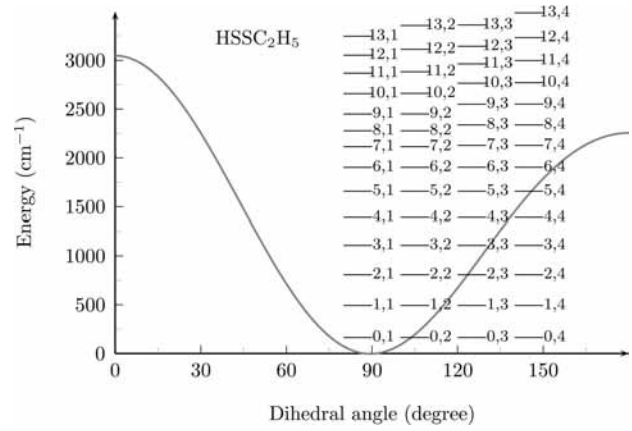

Figure 6. Torsional energy profile as a function of the dihedral angle and energy levels n and τ for $HSSC_2H_5$ (B3LYP method).

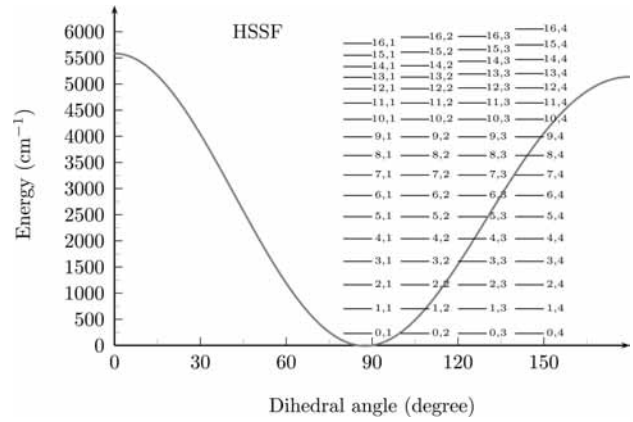

Figure 7. Torsional energy profile as a function of the dihedral angle and energy levels n and τ for HSSF (B3LYP method).

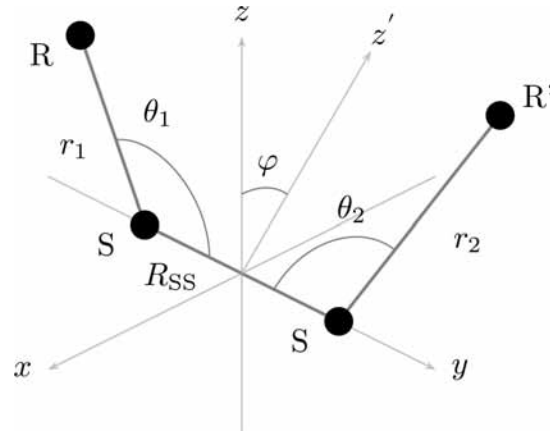

Figure 8. Illustration of the representation of the structure of the RSSR′ molecules in terms of the usual valence type of coordinates, where r_1, R_{SS}, and r_2 are the interatomic distances, θ_1 and θ_2 are the bond angles, and φ is the dihedral angle.

collisional mechanism for such processes.[38] We also estimated torsional levels and their populations as a function of temperature. With the results of the previous section, we can perform a similar study for H_2S_2 and its derivatives.

Interest in the specific features of torsional modes has been renewed recently; see, for example, refs 39−42 for spectroscopic investigations. With respect to the calculation of partition functions, of relevance both for thermodynamical and for reaction kinetic problems, see refs 43−48 and references therein. Partition functions are computed according to well-established formulas by explicit use of the calculated torsional levels and also by giving a test for simple classical and semiclassical approximations. In the calculation of the classical partition function, we found it important to consider a correction proposed in refs 49 and 50, which uses features of the linear approximation of the classical path (LCP) approach and the quadratic Feynman−Hibbs (QFH) approximation of the Feynman path integral.

An important aspect of the calculation of the classical torsional partition functions is the dependence of the moment of inertia on the geometrical parameters and on the dihedral angle. For discussions and calculations of the effective moment of inertia of molecules with internal rotation, see, for example, refs 46 and 51 and references therein. In previous work,[28] we tested alternative expressions for the moment of inertia, which can be considered as a constant only in a first approximation, and also considered a more general approach based on the kinetic energy operator, which takes into account the dependence from the dihedral angle, verifying that the explicit introduction of such a dependence from the dihedral angle improves the classical approximations for the torsional partition functions.

As for the peroxide cases,[28] the results presented in this paper allow us to characterize the racemization rates, which determine the process of stereomutation[52,53] between the two enantiomeric forms connected by torsion around the S−S bond. Computed level splittings provide the characteristic time for quantum mechanical tunneling, which is the mechanism responsible for the chirality changing process at low temperature, whereas for high temperature, the time of racemization is estimated by transition state theory using the computed partition functions.

Level Distribution. Data relevant to the present work are listed in Table 3 for the equilibrium, cis, and trans configurations. The calculated energy profiles along the torsional angle, φ, in the range from 0° (the cis configuration) to 180° (the trans configuration) with a step of 1°, optimizing the geometry at each angle, refer to the B3LYP method. The MP2(FU) results for the barriers proved that the less time-consuming density functional approach provided correct trends for the systematic investigation of intramolecular dynamics. The resulting values are fitted to a cosine expansion:

$$V(\phi) = \sum_k C_k \cos(k\varphi) \qquad (1)$$

where $k = 0, 1, 2,....$ The coefficients C_k obtained by a Newton−Raphson fitting to the calculated potential energy

TABLE 5: Distribution of the Levels for the H_2S_2 System, Evaluated with the MP2 Potential Curve

levels	temperature (K)					
n, τ	100	200	300	600	1000	2400
0, 1	0.249 416	0.237 784	0.216 051	0.154 325	0.105 394	0.049 292 667
0, 2	0.249 416	0.237 784	0.216 051	0.154 325	0.105 394	0.049 292 667
0, 3	0.249 416	0.237 784	0.216 051	0.154 325	0.105 394	0.049 292 666
0, 4	0.249 416	0.237 784	0.216 051	0.154 325	0.105 394	0.049 292 666
1, 1	0.000 582	0.011 490	0.028 662	0.056 209	0.057 496	0.038 293 554
1, 2	0.000 582	0.011 490	0.028 662	0.056 209	0.057 496	0.038 293 554
1, 3	0.000 582	0.011 490	0.028 662	0.056 209	0.057 496	0.038 293 543
1, 4	0.000 582	0.011 490	0.028 662	0.056 209	0.057 496	0.038 293 543
2, 1	0.000 002	0.000 672	0.004 320	0.021 822	0.032 591	0.030 227 201
2, 2	0.000 002	0.000 672	0.004 320	0.021 822	0.032 591	0.030 227 197
2, 3	0.000 002	0.000 672	0.004 320	0.021 821	0.032 590	0.030 226 801
2, 4	0.000 002	0.000 672	0.004 320	0.021 821	0.032 590	0.030 226 798
3, 1	0.000 000	0.000 049	0.000 754	0.009 115	0.019 303	0.024 300 582
3, 2	0.000 000	0.000 049	0.000 754	0.009 115	0.019 303	0.024 300 529
3, 3	0.000 000	0.000 049	0.000 752	0.009 103	0.019 290	0.024 292 143
3, 4	0.000 000	0.000 049	0.000 752	0.009 103	0.019 290	0.024 292 090
4, 1	0.000 000	0.000 005	0.000 160	0.004 204	0.012 133	0.020 025 820
4, 2	0.000 000	0.000 005	0.000 160	0.004 204	0.012 132	0.020 025 403
4, 3	0.000 000	0.000 005	0.000 153	0.004 114	0.011 975	0.019 917 277
4, 4	0.000 000	0.000 005	0.000 153	0.004 113	0.011 975	0.019 916 800
5, 1	0.000 000	0.000 001	0.000 048	0.002 307	0.008 465	0.017 236 934
5, 2	0.000 000	0.000 001	0.000 048	0.002 307	0.008 463	0.017 235 321
5, 3	0.000 000	0.000 001	0.000 036	0.001 985	0.007 734	0.016 600 321
5, 4	0.000 000	0.000 001	0.000 036	0.001 983	0.007 730	0.016 596 953
6, 1	0.000 000	0.000 000	0.000 016	0.001 333	0.006 091	0.015 027 826
6, 2	0.000 000	0.000 000	0.000 016	0.001 330	0.006 083	0.015 019 231
6, 3	0.000 000	0.000 000	0.000 009	0.000 971	0.005 037	0.013 883 774
6, 4	0.000 000	0.000 000	0.000 008	0.000 965	0.005 017	0.013 860 886
7, 1	0.000 000	0.000 000	0.000 004	0.000 676	0.004 053	0.012 682 327
7, 2	0.000 000	0.000 000	0.000 004	0.000 664	0.004 009	0.012 624 054
7, 3	0.000 000	0.000 000	0.000 002	0.000 480	0.003 300	0.011 640 645

points are given in Table 4. Illustrations of the distribution of levels obtained as described below are presented in Figures 5, 6, and 7 for the cases of the HSSH, $HSSC_2H_5$, and HSSF molecules, respectively. References 24−26 provide further details.

The effective kinetic energy operator that we have employed for the calculation of energy levels is of the type used, for example, by Likar at al[54] for HOOR systems. The present application is for general RSSR′ systems, where R and R′ can be an atom or a group of atoms. Coordinates are illustrated in Figure 8. The kinetic energy operator can be written in the Hermitian (self-adjoint) form:

$$\hat{T}(\varphi) = -\frac{\mathrm{d}}{\mathrm{d}\varphi}\,\alpha(\varphi)\,\frac{\mathrm{d}}{\mathrm{d}\varphi} = -\frac{\mathrm{d}}{\mathrm{d}\varphi}\left(\frac{\hbar^2}{2I(\varphi)}\right)\frac{\mathrm{d}}{\mathrm{d}\varphi} \qquad (2)$$

with

$$\alpha(\varphi) = \alpha_0 + \alpha_1 \cos\varphi \qquad (3)$$

$$\alpha_0 = \frac{1}{\mu_{RS}{r_1}^2 \sin^2\theta_1} + \frac{1}{\mu_{SR}{r_2}^2 \sin^2\theta_2} + \frac{1}{\mu_{SS}{R_{SS}}^2}(\cot^2\theta_1 + \cot^2\theta_2) - \frac{2}{m_S R_{SS}}\left(\frac{\cot\theta_1}{r_1 \sin\theta_1} + \frac{\cot\theta_2}{r_2 \sin\theta_2}\right) \qquad (4)$$

$$\alpha_1 = \frac{4\cot\theta_1 \cot\theta_2}{m_S{R_{SS}}^2} - \frac{2}{m_S R_{SS}}\left[\frac{\cot\theta_2}{r_1 \sin\theta_1} + \frac{\cot\theta_1}{r_2 \sin\theta_2}\right] \qquad (5)$$

where m_S is the sulfur mass and μ's are reduced masses. All the geometrical parameters (see Figure 8) are assumed to have their values as given in Table 3. These equations are obtained using the Appendix of ref 54 and the work of Decius[55] (equation for $g_{\tau\tau}{}^4$ on page 1028); see also ref 56. In eq 2, we have found it convenient to define an effective moment of inertia, I, as an explicit function of the torsional angle, φ.

$$I(\varphi) = \frac{\hbar^2}{2\alpha(\varphi)} \qquad (6)$$

The values of the α_0 and α_1 parameters are listed in Table 4. These formulas are reasonable approximations, provided that the variations of the other geometrical variables (bond lengths and bending angles) remain small as the dihedral angle varies. The choice of the equilibrium value for R_{SS} is appropriate for the low levels of relevance in this paper, but more accurate choices should be tested for the higher ones.

In view of the symmetry of the torsional potential by reflection with respect to φ equal to both 0 and π, corresponding

TABLE 6: First Levels of Each Symmetry in cm^{-1} [a]

molecule	n	
	0	1
HSSH DFT $\tau = 1, 2$	214.585	633.467
$\tau = 3, 4$	214.585	633.468
HSSH MP2	218.463	639.645
HSSF	229.068	700.427
HSSCl	202.566	613.784
FSSF	154.039	369.225
ClSSF	112.568	287.926
ClSSCl	81.410	218.691
$HSSCH_3$	163.324	480.871
$HSSC_2H_5$	164.298	493.048

[a] Calculated splitting are HSSH $\sim 4 \times 10^{-6}$ and $\sim 5 \times 10^{-6}$ (at DFT and MP2 levels, respectively), $HSSCH_3 \sim 2 \times 10^{-10}$, and $HSSC_2H_5 \sim 10^{-10}$.

TABLE 7: Torsional Partition Functions at Different Temperatures for the HSSH at DFT and MP2 Levels

	HSSH DFT					HSSH MP2				
T (K)	Q^{q}	$Q^{c}_{\alpha_0}$	Q^{c}_{α}	$Q^{sc}_{\alpha_0}$	Q^{sc}_{α}	Q^{q}	$Q^{c}_{\alpha_0}$	Q^{c}_{α}	$Q^{sc}_{\alpha_0}$	Q^{sc}_{α}
200	0.450	0.644	0.644	0.444	0.444	0.437	0.628	0.628	0.431	0.431
300	0.828	0.973	0.973	0.825	0.825	0.812	0.955	0.955	0.808	0.808
600	1.945	2.016	2.016	1.944	1.944	1.919	1.990	1.990	1.917	1.918
1000	3.508	3.544	3.545	3.507	3.508	3.464	3.501	3.502	3.464	3.464
2400	9.005	9.012	9.013	9.003	9.005	8.898	8.906	8.907	8.897	8.898

TABLE 8: Torsional Partition Functions at Different Temperatures for the HSSF and HSSCl Molecules

	HSSF					HSSCl				
T (K)	Q^{q}	$Q^{c}_{\alpha_0}$	Q^{c}_{α}	$Q^{sc}_{\alpha_0}$	Q^{sc}_{α}	Q^{q}	$Q^{c}_{\alpha_0}$	Q^{c}_{α}	$Q^{sc}_{\alpha_0}$	Q^{sc}_{α}
200	0.398	0.621	0.621	0.397	0.397	0.491	0.693	0.693	0.490	0.489
300	0.745	0.914	0.914	0.744	0.744	0.881	1.030	1.029	0.880	0.879
600	1.718	1.807	1.807	1.718	1.717	1.985	2.062	2.061	1.985	1.985
1000	2.987	3.040	3.039	2.988	2.987	3.464	3.509	3.507	3.465	3.464
2400	7.808	7.826	7.825	7.810	7.808	9.163	9.177	9.176	9.164	9.163

TABLE 9: Torsional Partition Functions at Different Temperatures for the ClSSCl, ClSSF and FSSF Molecules

	ClSSCl					ClSSF					FSSF				
T (K)	Q^{q}	$Q^{c}_{\alpha_0}$	Q^{c}_{α}	$Q^{sc}_{\alpha_0}$	Q^{sc}_{α}	Q^{q}	$Q^{c}_{\alpha_0}$	Q^{c}_{α}	$Q^{sc}_{\alpha_0}$	Q^{sc}_{α}	Q^{q}	$Q^{c}_{\alpha_0}$	Q^{c}_{α}	$Q^{sc}_{\alpha_0}$	Q^{sc}_{α}
200	1.772	1.860	1.846	1.787	1.772	1.240	1.331	1.324	1.247	1.240	0.838	0.928	0.925	0.842	0.838
300	2.799	2.872	2.851	2.821	2.799	2.042	2.114	2.104	2.052	2.042	1.479	1.552	1.547	1.485	1.479
600	5.836	5.903	5.863	5.876	5.836	4.403	4.457	4.437	4.423	4.403	3.391	3.442	3.431	3.403	3.391
1000	9.877	9.951	9.893	9.934	9.877	7.507	7.558	7.528	7.537	7.507	5.900	5.944	5.925	5.918	5.900
2400	24.886	24.869	24.892	24.863	24.886	18.530	18.569	18.538	18.561	18.530	14.593	14.635	14.604	14.624	14.593

TABLE 10: Torsional Partition Functions at Different Temperatures for the $HSSCH_3$ and $HSSC_2H_5$ Molecules

	$HSSCH_3$					$HSSC_2H_5$				
T (K)	Q^{q}	$Q^{c}_{\alpha_0}$	Q^{c}_{α}	$Q^{sc}_{\alpha_0}$	Q^{sc}_{α}	Q^{q}	$Q^{c}_{\alpha_0}$	Q^{c}_{α}	$Q^{sc}_{\alpha_0}$	Q^{sc}_{α}
200	0.689	0.848	0.848	0.686	0.686	0.678	0.847	0.847	0.675	0.675
300	1.175	1.289	1.288	1.174	1.174	1.152	1.272	1.272	1.151	1.151
600	2.625	2.680	2.680	2.625	2.625	2.552	2.610	2.610	2.552	2.552
1000	4.690	4.718	4.718	4.690	4.690	4.538	4.566	4.568	4.536	4.537
2400	12.100	12.103	12.106	12.097	12.100	11.785	11.788	11.792	11.781	11.785

to the two (cis and trans) planar configurations, the problem block-diagonalizes in four symmetry classes (Floquet's theorem), denoted by the quantum label $\tau = 1, 2, 3, 4$. Levels within each symmetry class are denoted by the quantum number $n = 0, 1, 2,....$ Traditional basis sets in terms of sine and cosine functions were used, giving rise to secular equations, in which the matrix elements are analytical integrals over trigonometric functions. So for each quantum number, n, there are the four well-known Mathieu symmetries ($\tau = 1, 2, 3, 4$), and the wave functions are correspondingly expanded in orthonormal trigonometric basis sets (see, e.g., ref 57).

Torsional Partition Functions. The level distribution as a function of temperature has been calculated (see also refs 25, 26, and 28) using the formula

$$\frac{N_{n\tau}}{N} = \frac{e^{-\beta E_{n\tau}}}{\sum_{n'\tau'} e^{-\beta E_{n'\tau'}}} \tag{7}$$

where $E_{n\tau}$ is the energy of the torsional state n and symmetry τ. As usual, $\beta = 1/K_B T$, where K_B is Boltzmann's constant and T is the temperature.

The quantum mechanical torsional partition function $Q^{q}(T)$ can be evaluated, at a given temperature, from the energies of the levels[44,58]

$$Q^{q}(T) = \sum_{n} \sum_{\tau=1,4} e^{-\beta E_{n\tau}} \tag{8}$$

According to previous work (see, e.g., refs 28 and 46), only levels having symmetries $\tau = 1$ and 4[57] are included.

At sufficiently high temperature, the quantum partition function can be usefully approximated by the classical expression[46,59,60]

$$Q^{c} = \sqrt{\frac{I}{2\pi\beta\hbar^2}} \int_0^{2\pi/\sigma} e^{-\beta V(\varphi)}\, d\varphi \tag{9}$$

(the T dependence is omitted from the notation for simplicity), where σ is an index number depending on the symmetric rotational group around the dihedral angle of the system; $\sigma = 1$ in our cases. Equation 9 implies that the torsional moment of inertia assumes a constant (effective or average) value.

Previously,[28] for ROOR′, we examined and assessed some improvements that do not spoil the basic requirement of simplicity of implementation. Since in general, I is related to the value of $\alpha(\varphi)$ according to eq 6, to calculate the moment of inertia from eq 6, as a first approximation, we consider only the α_0 term, neglecting α_1. Then

$$I = \frac{\hbar^2}{2\alpha_0} \tag{10}$$

and the expression (eq 9) can be written as

$$Q^{c}_{\alpha_0} = \sqrt{\frac{1}{4\pi\beta\alpha_0}} \int_0^{2\pi/\sigma} e^{-\beta V(\varphi)}\, d\varphi \tag{11}$$

However, accounting for the dependence of I and α on φ leads to an improved approximation inserting the explicit functional dependence under the integral sign

TABLE 11: Tunneling Splittings and Racemization Times[a]

				Q^q			τ_T			
system	E_{trans}	ΔE	τ_0	$T = 200$	$T = 300$	$T = 600$	$T = 2400$	$T = 200$	$T = 300$	$T = 600$	$T = 2400$
HSSH DFT	2010.183	3.6351×10^{-6}	4.5884×10^{-6}	0.450	0.828	1.945	9.005	$1.029\,65 \times 10^{-7}$	$1.018\,52 \times 10^{-9}$	$9.646\,82 \times 10^{-12}$	$3.004\,72 \times 10^{-13}$
HSSH MP2	2001.627	4.8613×10^{-6}	3.4310×10^{-6}	0.437	0.812	1.919	8.898	$9.402\,14 \times 10^{-8}$	$9.586\,83 \times 10^{-10}$	$9.324\,58 \times 10^{-12}$	$2.953\,83 \times 10^{-13}$
HSSF	5137.100			0.398	0.745	1.718	7.808	$5.353\,81 \times 10^{2}$	$2.985\,14 \times 10^{-3}$	$1.537\,88 \times 10^{-8}$	$1.698\,12 \times 10^{-12}$
HSSCl	3933.355			0.491	0.881	1.985	9.163	$1.145\,64 \times 10^{-1}$	$1.097\,93 \times 10^{-5}$	$9.909\,58 \times 10^{-10}$	$9.684\,25 \times 10^{-13}$
FSSF	10926.858			0.838	1.479	3.391	14.593	$1.382\,72 \times 10^{21}$	$6.790\,76 \times 10^{9}$	$3.249\,36 \times 10^{-2}$	$1.020\,86 \times 10^{-10}$
ClSSF	8241.282			1.240	2.042	4.403	18.530	$8.326\,73 \times 10^{12}$	$2.389\,90 \times 10^{4}$	$6.736\,06 \times 10^{-5}$	$2.591\,16 \times 10^{-11}$
ClSSCl	6199.415			1.772	2.799	5.836	24.886	$4.968\,12 \times 10^{6}$	$1.829\,97 \times 100$	$6.673\,15 \times 10^{-7}$	$1.023\,21 \times 10^{-11}$
$HSSCH_3$	2105.658	2×10^{-10}	0.08	0.689	1.175	2.625	12.100	$3.133\,17 \times 10^{-7}$	$2.284\,74 \times 10^{-9}$	$1.636\,91 \times 10^{-11}$	$4.275\,27 \times 10^{-13}$
$HSSC_2H_5$	2255.503	1×10^{-10}	0.17	0.678	1.152	2.552	11.785	$9.060\,58 \times 10^{-7}$	$4.595\,78 \times 10^{-9}$	$2.279\,44 \times 10^{-11}$	$4.555\,35 \times 10^{-13}$

[a] ΔE and E_{trans} are in cm^{-1}; τ_0 and τ_T are in seconds.

$$Q_\alpha^c = \sqrt{\frac{1}{4\pi\beta}} \int_0^{2\pi/\sigma} \frac{e^{-\beta V(\varphi)}}{(\alpha_0 + \alpha_1 \cos\varphi)^{1/2}}\, d\varphi \qquad (12)$$

This expression provides a more general equation for the calculation of the classical partition function, that has been shown[28] to lead to improved accurate results.

We have also calculated the partition function semiclassically using the formulation proposed in refs 49 and 50. (For a systematic discussion of alternatives, see ref 46). This method uses features of the linear approximation of the classical path approach and the quadratic Feynman−Hibbs approximation to the Feynman path integral. This LCP/QFH hybrid approach, which we denote by the superscript SC for "semiclassical", consists of using in eqs 9, 11, and 12, instead of $V(\varphi)$, the following effective potential,

$$V(\varphi) \rightarrow V(\varphi) + \frac{\hbar^2\beta}{48I}\left[\frac{d^2}{d\varphi^2} V(\varphi) + \beta\left(\frac{d}{d\varphi} V(\varphi)\right)^2\right] \qquad (13)$$

where I is the moment of inertia. When I is calculated using only α_0, eq 11, we have an approximation that we denote $Q_{\alpha_0}^{sc}$, whereas when using eq 6, which accounts for the dihedral angle dependence, we have the approximation that we denote as Q_α^{sc}.

5. Results and Discussion

To provide the torsional potential curves, we have calculated the coefficients of the expansion (see eq 1) for maximum $k = 6$ for all systems (HSSH, HSSF, HSSCl, $HSSCH_3$, $HSSC_2H_5$) except ClSSCl, ClSSF, and FSSF, for which k up to 8 was needed to minimize the root mean square (rms) deviation,

$$\mathrm{RMS} = \sqrt{\frac{1}{N}\sum_{i=1}^{N}\left[V^0(\varphi_i) - V(\varphi_i)\right]^2} \qquad (14)$$

where V^0 is the potential energy calculated by quantum mechanical methods and V is the fitted potential at the dihedral angle, φ_i. The total number, N, was determined by the available grid points, which are spaced by 1°. The coefficients of the expansion (eq 1) are shown in Table 4.

In the following, we discuss the effects of the substituents on the potential energy profile of the torsional mode. The structural parameters and cis and trans barriers for all systems that we have considered are shown in Table 3.

Hydrogen Disulfide. In a previous article, we presented calculated torsional levels for H_2O_2. For the H_2S_2 molecule, the torsional potential and the levels distribution are shown in Figure 5. In particular, to study the statistical thermodynamics of torsional modes, we have calculated their temperature distributions and the torsional partition functions. Table 5 shows the level distributions as a function of the temperature for the H_2S_2 molecule, recently reinvestigated.[29]

In Table 7, we list the torsional partition function at different temperatures for the H_2S_2 system. Q^q is calculated using eq 8 directly from the levels of the symmetries $\tau = 1$ and $\tau = 4$ (see above for this choice). For $Q_{\alpha_0}^c$, we use eq 11, and for Q_α^c, we use eq 10. Finally, $Q_{\alpha_0}^{sc}$ and Q_α^{sc} are calculated using the semiclassical, or LCP/QFH approach described at the end of Torsional Partition Functions. From the results of Table 7, one notes that this approach introduces a substantial improvement in comparison with the classical one, even for low temperatures.

Other Systems. As is known, the features of the distribution of the torsional levels depend on the potential profile (trans and cis barriers) and of the masses of the atoms (moment of inertia). For this, we are looking at the results for the other disulfide

systems. One notes that the lowest levels, one for each of the four symmetries,[57] are nearly degenerate ($n = 0$, $\tau = 1, 2, 3, 4$), as shown in Figure 6 and Table 6. That is due to tunneling being hindered by both heavier masses and higher barriers. Increasing n, this behavior persists under the lowest (trans) barrier, in proximity of which the degeneracy between the first two symmetries ($\tau = 1$ and 2) and the other two ($\tau = 3$ and 4), is removed. Going up in energy, the levels encounter the higher (cis) barrier, and here, the effect on the symmetry is different. The energy of the first symmetry increases more slowly than the others so that in the high energy limit, it becomes degenerate with the fourth symmetry of the previous layer; at the same time, the levels with $\tau = 2$ and 3 symmetries become degenerate. For energies close to the two barrier tops, we notice an accumulation of states, typical of the anharmonicity of the potentials. An example of this behavior is shown in Figure 6 for the $HSSC_2H_5$ molecule. Figure 7 exhibits the case of HSSF, in which the cis and trans barriers are approximately of the same height.

In Table 8, we report the partition functions at various temperatures for the HSSF and HSSCl systems. In Table 9, the partition functions at various temperatures for the ClSSCl, ClSSF, and FSSF molecules. In Table 10, we list the partition functions at various temperatures for the $HOOCH_3$ and $HOOC_2H_5$ molecules. Q^q are calculated using eq 8 directly, as before, using the levels of symmetries $\tau = 1$ and $\tau = 4$ only. Again, for $Q^c_{\alpha_0}$ and for Q^c_α, we use eqs 11 and 12. $Q^{sc}_{\alpha_0}$ and Q^{sc}_α were again calculated using the semiclassical or the LCP/QFH approach described at the end of Torsional Partition Functions. In addition, in these cases, we obtain a substantial improvement. In all systems presented here, the agreement between the results of the semiclassical Q^{sc}_α and quantum Q^q procedures is excellent, even for the lowest temperatures presented. This indicates that the semiclassical procedure, or LCP/QFH approach, turns out to be extremely accurate. Furthermore, the use of the moment of inertia as a function of φ does not lead to significant improvement in disulfide systems, which is different from what was found in the previous study[28] for the molecules containing the peroxidic bonds. Exceptions are observed for ClSSCl, ClSSF, and FSSF.

Intramolecular Chirality Changing Rates. As an important application of the results of previous sections, Table 11 shows the tunnel splittings and racemization times for some of the investigated systems in the spirit of Quack and co-workers.[53] The tunneling time is calculated directly from the level splitting of the symmetries $\tau = 1$ and $\tau = 4$ using the two-level equation and the Heisenberg uncertainty principle.

$$\tau_0 \simeq \frac{h}{2\Delta E} \tag{15}$$

This can be interpreted as a racemization time at very low temperatures where only the ground state is populated. In the opposite limit of high temperature, the racemization time is modeled as occurring by passage over the trans barrier using transition state theory with no tunneling correction,[53]

$$\tau_T \simeq \frac{h}{2k_B T}\, Q^q(T) \exp(E_{trans}/k_B T) \tag{16}$$

where E_{trans} is the trans barrier height (lower than the cis in the cases considered here, Table 3), k_B the Boltzmann's constant, and $Q^q(T)$ the partition function for the torsional mode (see eq 8).

It can be observed in Table 11 that racemization times, for both low (τ_0) and high (τ_T) temperatures, can be quite high, reaching the order of seconds (or more) for some molecules containing the S−S bond. This behavior is related to the height of the trans barriers, which for the disulfides presented in Table 3 are always on the same order of magnitude as the cis barriers. The reader will find it interesting to compare the results in Table 11 to those reported in the corresponding Table 9 of ref 28 for ROOR′ molecules, in which rates were generally much smaller because of the much smaller trans barriers.

6. Further Remarks and Conclusion

The investigation presented in this paper of properties of a series of molecules containing the −SS− bond has been focused mainly on the role in the intramolecular dynamics of the energy profile along the torsional mode. We hope to have exhibited some general trends that may assist further theoretical and eventually experimental approaches aimed at understanding the possible role of chirality-changing phenomena, both in intramolecular and possibly in intermolecular processes, the latter induced by collisions and to be investigated by characterizing intermolecular interactions (see ref 29 for HSSH).

Along the line that we have pursued for the analogous series of molecules containing the −OO− bond, we have computed the temperature dependence of energy levels and the partition functions, useful to estimate racemization rates. Not unexpectedly, the latter are, in general, smaller than for the −OO− series of molecules,[28] and span several orders of magnitudes, offering a very ample phenomenology for dedicated experimental exploration.

Acknowledgment. This research is supported by a PRIN Grant from the Italian Ministry for University and Scientific and Technological Research and by ASI (Agenzia Spaziale Italiana). A.C.P.B. acknowledges a CAPES fellowship. F.V.P. thanks CNPq (Brazil) for financial support.

References and Notes

(1) Cárdenas-Jirón, G. I.; Toro-Labbé, A. *J. Mol. Struct. (THEOCHEM)* **1997**, *390*, 79.
(2) Bergés, J.; Rickards, G.; Rauk, A.; Houée-Levin, C. *Chem. Phys. Lett.* **2006**, *421*, 63.
(3) Rickard, G. A.; Bergés, J.; Houée-Levin, C.; Rauk, A. *J. Phys. Chem. B* **2008**, *112*, 5774.
(4) Zysman-Colman, E.; Harp, D. N. *J. Sulfur Chem.* **2004**, *24*, 291.
(5) Grabowski, J. J.; Zhang, L. *J. Am. Chem. Soc.* **1989**, *111*, 1193.
(6) Marsden, C. J.; Oberhammer, H.; Lösking, O.; Willner, H. *J. Mol. Struct (THEOCHEM)* **1989**, *193*, 233.
(7) Dolenko, G. N.; Deryagina, E. N.; Turchaninova, L. P.; Elin, V. P.; Basina, E. I.; Pavlova, T. O.; Voronov, V. K. *J. Heteroat. Chem.* **1995**, *6*, 623.
(8) Cheng, B.-M.; Hung, W.-C. *J. Phys. Chem.* **1996**, *100*, 10210.
(9) Cao, X.; Qiao, C.; Wang, D. *Chem. Phys. Lett.* **1998**, *290*, 405.
(10) Marsden, C. J.; Smith, B. J. *J. Phys. Chem.* **1988**, *92*, 347.
(11) Bickelhaupt, F. M.; Solà, M.; Schleyer, P. v. R. *J. Comp. Chem.* **1995**, *16*, 465.
(12) Cardenas-Jiron, G. I.; Lahsen, J.; Toro-Labbé, A. *J. Phys. Chem.* **1995**, *99*, 5325.
(13) Koput, J. *Chem. Phys. Lett.* **1996**, *259*, 146.
(14) Altmann, J.; Handy, N. C.; Ingamells, V. E. *Int. J. Quantum Chem.* **1996**, *57*, 533.
(15) Jursic, B. R. *J. Comput. Chem.* **1996**, *17*, 835.
(16) Steudel, R.; Drozdova, Y.; Miaskiewicz, K.; Hertwig, R. H.; Koch, W. *J. Am. Chem. Soc.* **1997**, *119*, 1990.
(17) Das, D.; Whittenburg, S. L. *J. Phys. Chem. A* **1999**, *103*, 2134.
(18) Braida, B.; Hiberty, P. C. *J. Phys. Chem. A* **2003**, *107*, 4741.
(19) Ball, D. W. *J. Mol. Struct. (THEOCHEM)* **2004**, *676*, 15.
(20) Prascher, B. P.; Wilson, A. K. *J. Mol. Struct. (THEOCHEM)* **2007**, *814*, 1.
(21) Ornellas, F. R. *Chem. Phys. Lett.* **2007**, *448*, 24.
(22) Zeng, Y.; Li, X.; Zhang, X.; Zheng, S.; Meng, L. *J. Mol. Struct. (THEOCHEM)* **2008**, *851*, 115.
(23) Dumont, E.; Loos, P.-F.; Assfeld, X. *Chem. Phys. Lett.* **2008**, *458*, 276.

(24) Maciel, G. S.; Bitencourt, A. C. P.; Ragni, M.; Aquilanti, V. *Chem. Phys. Lett.* **2006**, *432*, 383.
(25) Maciel, G. S.; Bitencourt, A. C. P.; Ragni, M.; Aquilanti, V *Int. J. Quantum Chem.* **2007**, *107*, 2697.
(26) Maciel, G. S.; Bitencourt, A. C. P.; Ragni, M.; Aquilanti, V. *J. Phys. Chem. A* **2007**, *111*, 12604.
(27) Barreto, P. R. P.; Vilela, A. F. A.; Lombardi, A.; Maciel, G. S.; Palazzetti, F.; Aquilanti, V. *J. Phys. Chem. A* **2007**, *111*, 12754.
(28) Bitencourt, A. C. P.; Ragni, M.; Maciel, G. S.; Aquilanti, V.; Prudente, F. *J. Chem. Phys.* **2008**, *129*, 154316.
(29) Maciel, G. S.; Barreto, P. R. P.; Lombardi, A.; Palazzetti, F.; Aquilanti, V. *J. Chem. Phys.* **2008**, *129*, 164302.
(30) Cappelletti, D.; Aquilanti, V.; Cornicchi, E.; Teixidor, M. M.; Pirani, F. *J. Chem. Phys.* **2005**, *123*, 024302.
(31) Aquilanti, V.; Cornicchi, E.; Teixidor, M. M.; Saendig, N.; Pirani, F.; Cappelletti, D. *Angew. Chem. Int.* **2005**, *Ed. 44*, 2356.
(32) Cappelletti, D.; Vilela, A. F. A.; Barreto, P. R. P.; Gargano, R.; Pirani, F.; Aquilanti, V. *J. Chem. Phys.* **2006**, *125*, 133111.
(33) Aquilanti, V.; Cappelletti, D.; Pirani, F.; Roncaratti, L. *Int. J. Mass. Spectrom.* **2008**, in press.
(34) Frisch, M. J. et al. *Gaussian 03*, Revision C.02; Gaussian, Inc.: Wallingford, CT, 2004.
(35) Sing, U. C.; Kollman, P. *J. Comput. Chem.* **1984**, *5*, 129.
(36) Maciel, G.; Garcia, E. *Chem. Phys. Lett.* **2005**, *409*, 29.
(37) Winnewisser, B. P.; Winnewisser, M.; Medvedev, I. R.; Behnke, M.; De Lucia, F. C.; Ross, S. C.; Koput, J. *Phys. Rev. Lett.* **2005**, *95*, 243002.
(38) Aquilanti, V.; Maciel, G. S. *Orig. Life Evol. Biosph.* **2006**, *36*, 435.
(39) Pelz, G.; Yamada, K. M. T.; Winnewisser, G. *J. Mol. Spectrosc.* **1993**, *159*, 507.
(40) Yamada, K. M. T.; Winnewisser, G.; Jensen, P. *J. Mol. Struct.* **2004**, *695*, 323.
(41) Bakasov, A.; Berger, R.; Ha, T.-K.; Quack, M. *Int. J. Quantum Chem.* **2004**, *99*, 393.
(42) Ross, S. C.; Yamada, K. M. T. *Phys. Chem. Chem. Phys.* **2007**, *9*, 5809.
(43) Chuang, Y.-Y.; Truhlar, D. G. *J. Chem. Phys.* **2000**, *112*, 1221; **2004**, *121*, 7036(E); **2006**, *124*, 179903(E).
(44) Lynch, V. A.; Mielke, S. L.; Truhlar, D. G. *J. Chem. Phys.* **2004**, *121*, 5148.
(45) Lynch, V. A.; Mielke, S. L.; Truhlar, D. G *J. Phys. Chem. A* **2005**, *109*, 10092; **2006**, *110*, 5965. .
(46) Ellingson, B. A.; Lynch, V. A.; Mielke, S. L.; Truhlar, D. G. *J. Chem. Phys.* **2006**, *125*, 084305.
(47) Sturdy, Y. K.; Clary, D. C. *Phys. Chem. Chem. Phys.* **2007**, *9*, 2065.
(48) Sturdy, Y. K.; Clary, D. C. *Phys. Chem. Chem. Phys.* **2007**, *9*, 2397.
(49) Prudente, F. V.; Riganelli, A.; Varandas, A. J. C. *J. Phys. Chem. A* **2001**, *105*, 5272.
(50) Prudente, F. V.; Varandas, A. J. C. *J. Phys. Chem. A* **2002**, *106*, 6193.
(51) Pitzer, K. S.; Gwinn, W. D. *J. Chem. Phys.* **1942**, *10*, 428.
(52) Quack, M.; Willeke, M. *J. Phys. Chem. A* **2006**, *110*, 3338.
(53) Fehrensen, B.; Luckhaus, D.; Quack, M. *Chem. Phys.* **2007**, *338*, 90.
(54) Likar, M. D.; Baggott, J. E.; Crim, F. F. *J. Chem. Phys.* **1989**, *90*, 6266.
(55) Decius, J. C. *J. Chem. Phys.* **1948**, *16*, 1025.
(56) Wilson, E. B., Jr.; Decius, J. C.; Cross, P. C. *Molecular Vibrations*; Dover Publications, Inc.: New York, 1980.
(57) Hunt, R. H.; Leacock, R. A.; Peters, C. W.; Hecht, K. T. *J. Chem. Phys.* **1965**, *42*, 1931.
(58) Riganelli, A.; Prudente, F. V.; Varandas, A. J. C. *Phys. Chem. Chem. Phys.* **2000**, *18*, 4121.
(59) Riganelli, A.; Prudente, F. V.; Varandas, A. J. C. *J. Phys. Chem. A* **2001**, *105*, 9518.
(60) Urbano, A. P. A.; Prudente, F. V.; Riganelli, A.; Varandas, A. J. C. *Phys. Chem. Chem. Phys.* **2001**, *3*, 5000.
(61) Kushner, L. M.; Gorin, G.; Smith, C. P. *J. Am. Chem. Soc.* **1950**, *73*, 477.

JP8094215